$$\begin{cases} m_2\ddot{y}_2(t)+f_{c2}\left(\dot{z}_2(t)\right)+f_{k2}\left(z_2(t)\right)=0 \\ m_1\ddot{y}_1(t)+f_{c1}\left(\dot{z}_1(t)\right)+f_{k1}\left(z_1(t)\right)=f_{c2}\left(\dot{z}_2(t)\right)+f_{k2}\left(z_2(t)\right) \\ m_0\ddot{y}_0(t)+c_0\dot{y}_0(t)+k_0\left(y_0(t)-u(t)\right)=f_{c1}\left(\dot{z}_1(t)\right)+f_{k1}\left(z_1(t)\right) \end{cases}, \tag{3}$$

where $z_i(t)=y_i(t)-y_{i-1}(t)\ \ (i=1,2)$ and $\{m_i,\ c_i,\ k_i,\ y_i\ (i=1,2)\}$ is the set of mass, damping coefficient, stiffness and displacement on the ith storey, respectively. When this controlled system can be regarded as a linear system: $f_{ci}\left(z_i(t)\right)=c_i\dot{z}_i,\ f_{ki}\left(z_i(t)\right)=k_i z_i\ \ (i=1,2)$, its notations in the Laplace domain can be expressed by

$$\begin{cases} G_2(s)=\dfrac{y_2(s)}{y_1(s)}=\dfrac{c_2s+k_2}{m_2s^2+c_2s+k_2} \\ G_1(s)=\dfrac{y_1(s)}{y_0(s)}=\dfrac{\left(c_1s+k_1\right)}{\left(m_1s^2+\left(c_2+c_1\right)s+k_2+k_1\right)-\left(c_2s+k_2\right)G_2(s)} \\ G_0(s)=\dfrac{y_0(s)}{u(s)}=\dfrac{k_0}{\left(m_0s^2+\left(c_0+c_1\right)s+\left(k_0+k_1\right)\right)-\left(c_1s+k_1\right)G_1(s)} \end{cases}, \tag{4}$$

where G_i (i=0,1,2) is the transfer function describing the relation between y_i and y_{i-1}, though y_{-1} is equivalent to u. The top of the amplification device, which is the point to be controlled, is referred to as controlled point in this study. Then, the output of the controlled point is expressed by

$$y_2(s)=G_{cp}(s)u(s)=\frac{G_{cp}(s)}{s^2}\ddot{u}(s), \tag{5}$$

where $G_{cp}(s)=G_2(s)G_1(s)G_0(s)$.

The linear model of the controlled system is expressed by

$$\begin{cases} \bar{G}_2(s)=\dfrac{\bar{y}_2(s)}{\bar{y}_1(s)}=\dfrac{\bar{c}_2s+\bar{k}_2}{\bar{m}_2s^2+\bar{c}_2s+\bar{k}_2} \\ \bar{G}_1(s)=\dfrac{\bar{y}_1(s)}{\bar{y}_0(s)}=\dfrac{\left(\bar{c}_1s+\bar{k}_1\right)}{\left(\bar{m}_1s^2+\left(\bar{c}_2+\bar{c}_1\right)s+\bar{k}_2+\bar{k}_1\right)-\left(\bar{c}_2s+\bar{k}_2\right)\bar{G}_2(s)} \\ \bar{G}_0(s)=\dfrac{\bar{y}_0(s)}{u(s)}=\dfrac{\bar{k}_0}{\left(\bar{m}_0s^2+\left(\bar{c}_0+\bar{c}_1\right)s+\left(\bar{k}_0+\bar{k}_1\right)\right)-\left(\bar{c}_1s+\bar{k}_1\right)\bar{G}_1(s)} \end{cases}. \tag{6}$$

where $\{\bar{m}_i,\ \bar{c}_i,\ \bar{k}_i,\ \bar{y}_i\ \ (i=0,\ 1,2)\}$ is the set of mass, damping coefficient, stiffness and displacement on the ith

storey of the linear model, respectively. Then, the output of the linear model, corresponding to the controlled point, is expressed by

$$\bar{y}_2(s) = \bar{G}_{cp}(s)u(s) = \frac{\bar{G}_{cp}(s)}{s^2}\ddot{u}(s), \tag{7}$$

where $\bar{G}_{cp}(s) = \bar{G}_2(s)\bar{G}_1(s)\bar{G}_0(s)$.

In NSBC, the nonlinear signal σ is an essential factor and this signal in this study can be obtained by

$$\sigma(s) = y_2(s) - \bar{y}_2(s). \tag{8}$$

Based on Eq. (8), the error signal e between the reference signal r and y_2 can be expressed as

$$e(s) = r(s) - y_2(s) = r(s) - \bar{y}_2(s) - \sigma(s) = r(s) - \bar{G}_{cp}(s)e^{-\bar{\tau}s}u(s) - \sigma(s) \tag{9}$$

where $\bar{\tau}$ is the estimation delay associated with the linear model, while τ in Fig. 2 is the actual pure time delay associated with the controlled system.

At displacement control, the control input of NSBC is determined by

$$u(s) = K_r(s)r(s) + K_e(s)e(s) + K_\sigma(s)\sigma(s). \tag{10}$$

where K_r, K_e and K_σ are controllers acting on r, e, and σ, respectively. Substituting Eq. (10) into Eq. (9), the error signal can be rewritten as

$$e(s) = \frac{1 - \bar{G}_{cp}(s)e^{-\bar{\tau}s}K_r(s)}{1 + \bar{G}_{cp}(s)e^{-\bar{\tau}s}K_e(s)}r(s) - \frac{1 + \bar{G}_{cp}(s)e^{-\bar{\tau}s}K_\sigma(s)}{1 + \bar{G}_{cp}(s)e^{-\bar{\tau}s}K_e(s)}\sigma(s). \tag{11}$$

To achieve zero error in Eq. (11), particularly for $\tau = 0$, suitable controller transfer functions are found to be

$$\begin{cases} K_r(s) = \dfrac{1}{\bar{G}_{cp}(s)}F_r(s) \\ K_\sigma(s) = \dfrac{-1}{\bar{G}_{cp}(s)}F_\sigma(s), \\ K_e(s) = \dfrac{1}{\bar{G}_{cp}(s)}F_e(s) \end{cases} \tag{12}$$

where F_r, F_e and F_σ are the filters associated with the controllers acting on r, e, and σ, respectively. Common digital filter such as Butterworth filters are possible choices for F_r and F_σ. According to a study on NSBC [7], the filter F_e is expected to be

$$F_e(s) = \frac{\omega_e^2}{s^2 + 2\zeta_e \omega_e s}, \tag{13}$$

where $\{\omega_e, \zeta_e\}$ is the set of the cut-off frequency and damping ratio of the filter F_e, respectively.

Although the controller design above is for displacement control, its design can be simply extended to acceleration control by rewiring Eq. (10) as

$$u(s) = K_r'(s)\ddot{r}(s) + K_e'(s)\ddot{e}(s) + K_\sigma'(s)\ddot{\sigma}(s). \tag{14}$$

where $K_r'(s) = \frac{K_r(s)}{s^2}$, $K_e'(s) = \frac{K_e(s)}{s^2}$ and $K_\sigma'(s) = \frac{K_\sigma(s)}{s^2}$.

3. Numerical simulations

This section numerically examines the performance of NSBC for shaking table tests using an amplification device. This numerical examination employs various conditions of the E-Defense test that was performed for a high-rise building under a long-period ground motion. The E-Defense test was based on a 30-storey high-rise building and the long period ground motion, referred to as Higashi-yuuenchi ground motion [2]. This ground motion was artificially synthesized for an anticipated Nankai earthquake (M8.4), with a rupture length of 180 km and a focus depth of 10 km. In a numerical simulation, the high-rise building was modelled by a lumped mass model having nonlinear characteristic in each story stiffness. The model under the ground motion displayed inelastic behaviour and its third storey reached to the ductility factor of 4.1. In the E-Defense test, the target responses were made by the top floor's responses.

As the target response in this study, we also use a top-floor response of the 30-storey lumped mass model subjected to the long-period ground motion. E-Defense shaking table has various limitations such as acceleration, velocity and displacement [1]. However, focusing on the accuracy of the realized response on an amplification device, this study does not reflect such limitations to the examination of NSBC.

3.1 Numerical conditions

Numerical simulations here are performed for the 3DOF model shown in Fig. 3(b). The top 2DOF system demonstrates the five-storey rigid frame and amplification device, while the bottom SDOF system demonstrates the shaking table. The table has the following properties: m_0 = 750 ton, c_0 = 94.2 kNs/mm, and k_0 = 2961.0 kN/mm, which result in $\omega_0 = 10.0 \times 2\pi$ rad/s and $\zeta_0 = 1.0$ when the amplification device is not placed on the table. The parameters of the amplification device are set to $\{m_1, m_2\} = \{395, 360\}$ ton, $\{c_1, c_2\} = \{0.10,$

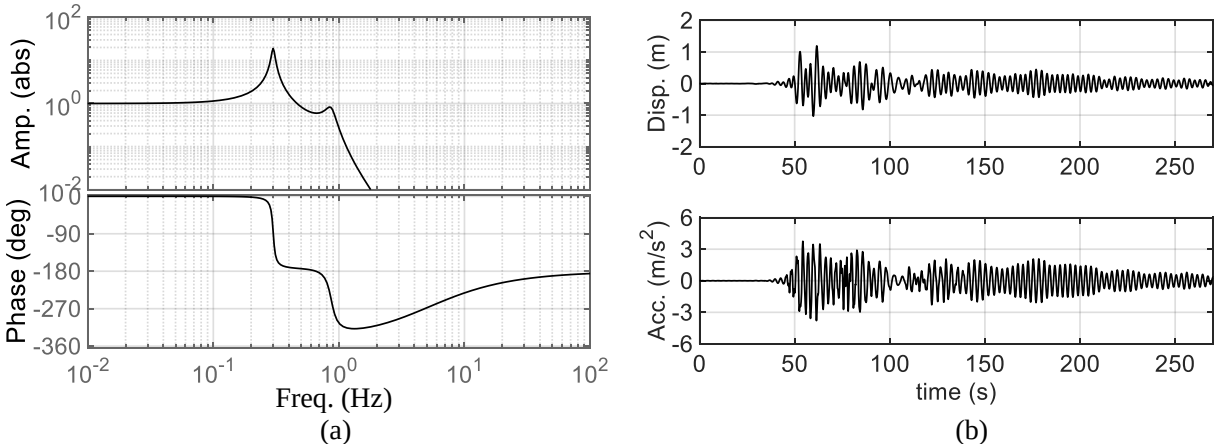

(a) (b)

Fig. 4. Numerical conidiations: (a) performance of amplification device, (b) target response.

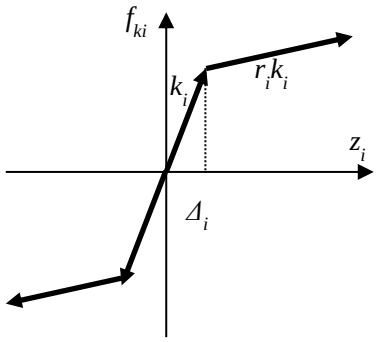

Fig. 5. Nonlinear characteristics of the *i*th spring.

0.15} kNs/mm, and $\{k_1, k_2\}=\{3.14, 4.79\}$ kN/mm, which derive from the E-Defense test [2,3,4].

Based on these parameters and the transfer function for the top of the device and the shaking table : $y_2(s)/y_0(s)=G_2(s)G_1(s)$, the performance of the amplification device can be illustrated as shown in Fig. 4(a). According to Fig. 4(a), the amplification device is mainly effective at the frequency of 0.3 Hz, while it is not over 1.0 Hz. This indicates that the target response containing higher frequency than 1.0 Hz is not suitable for this amplification device. Thus, the response in Fig. 4(b), which is processed by the second order high-pass Butterworth filter with the cut-off frequency of 1.0 Hz, is taken as the target response to be reproduced in this study.

According to a report on the E-Defense test [4], the rubber bearings used in the amplification device displayed nonlinear characteristics. Thus, this study also employs the nonlinearity in Fig. 5 into the spring on each storey of the 2DOF model, which mainly demonstrates the amplification device. This nonlinearity can be described by

$$F_{ki}\left(z_i(t)\right)=\begin{cases} k_i z_i \\ k_i\Delta_i \operatorname{sgn}\left(z_i\right)+r_i k_i\left(\delta_i-\Delta_i \operatorname{sgn}\left(z_i\right)\right) \end{cases}, \tag{15}$$

where Δ_i is the elastic limit of the spring on the *i*th layer, r_i is the reduction parameter associated *i*th spring, and $\operatorname{sgn}(a)=\{1\,(a>0),\ 0\,(a=0),\ -1\,(a<0)\}$. In this study, elastic limits of the nonlinear springs are fixed to be $\Delta_1=\Delta_2=0.1$ m, while the reduction parameters of the springs (i.e. r_1, r_2) is taken as a variable to tune the severity of nonlinear characteristics. In the following simulations, the reduction parameters are changed to be $r_1=r_2=0.9, 0.8, 0.7, 0.6, 0.5$. The pure time delay and its estimation delay required for NSBC are fixed to be $\bar{\tau}=\tau=10.0$ ms.

The reproduction accuracy of target acceleration is evaluated by the maximum error between the target and realized acceleration as well as its similarity between the two signals. This similarity is evaluated by

$$S_f=\left(1+\frac{\sum A_e(f)^2}{\sum A_r(f)^2}\right)^{-1}\times 100\%, \tag{16}$$

where A_r and A_e are the Fourier amplitude spectra of the reference signal *r* and the error signal *e*, respectively. S_f is evaluated within the range of 0.01–20.0 Hz.

3.2 Numerical results

The NSBC controllers are designed by the premise that all parameters of the controlled system within the elastic range is perfectly known. Thus, the transfer function $\bar{G}_{cp}(s)$ are simply built by employing the parameters given in 3.1 into Eq. (6): $\{\bar{m}_1, \bar{m}_2\} = \{m_1, m_2\}$, $\{\bar{c}_1, \bar{c}_2\} = \{c_1, c_2\}$ and $\{\bar{k}_1, \bar{k}_2\} = \{k_1, k_2\}$. For acceleration control, the controllers in NSBC here are designed by Eqs. (12) and (14). F_r and F_σ are designed as the second order Butterworth filter with the cut-off frequency of 20.0 Hz, and F_e is designed as Eq. (14) with ω_e=20·2π rad/s and ζ_e =1.0. These controllers are employed in NSBC and there are four types of practices in NSBC. The first practice is the feed-forward controller only: $\{K_r\}$. The other two practices are an addition of one feedback controller K_σ or K_e to the first application: $\{K_r, K_\sigma\}$ and $\{K_r, K_e\}$. The last practice is the addition of feedback controllers K_σ and K_e to the first application: $\{K_r, K_\sigma, K_e\}$. This study numerically examines these four types of practices for the controlled system having nonlinear characteristics.

When the controlled system does not have any nonlinear characteristics, which corresponds to the case of $r_1 = r_2 = 1.0$, the practice $\{K_r\}$ without any feedback actions have achieved perfect reproduction of the target response. However, the practice $\{K_r\}$ shows larger error and lower similarity, as the reduction parameter becomes lager, as shown in Fig. 6(a, b). Thus, the practice $\{K_r\}$ is found to be inadequate for systems having nonlinear characteristics. According to Fig. 6(a, b), the addition of a feedback action: the practices of $\{K_r, K_\sigma\}$ and $\{K_r, K_e\}$ have greatly improved the reproduction accuracy; the practice $\{K_r, K_\sigma\}$ shows slightly better results than the practice $\{K_r, K_\sigma\}$. The practice employing both feedback actions: $\{K_r, K_\sigma, K_e\}$ is found to produce the highest accuracy in the comparison with other practices, and this practice has resulted in near 100% similarity in all cases of $r_1 = r_2 = 0.9 - 0.5$.

According to Fig. 6(a, b), NSBC is found to be very effective to accurately reproduce the target response on the amplification device having nonlinear characteristics. However, as seen in Fig. 6(c), the shaking table

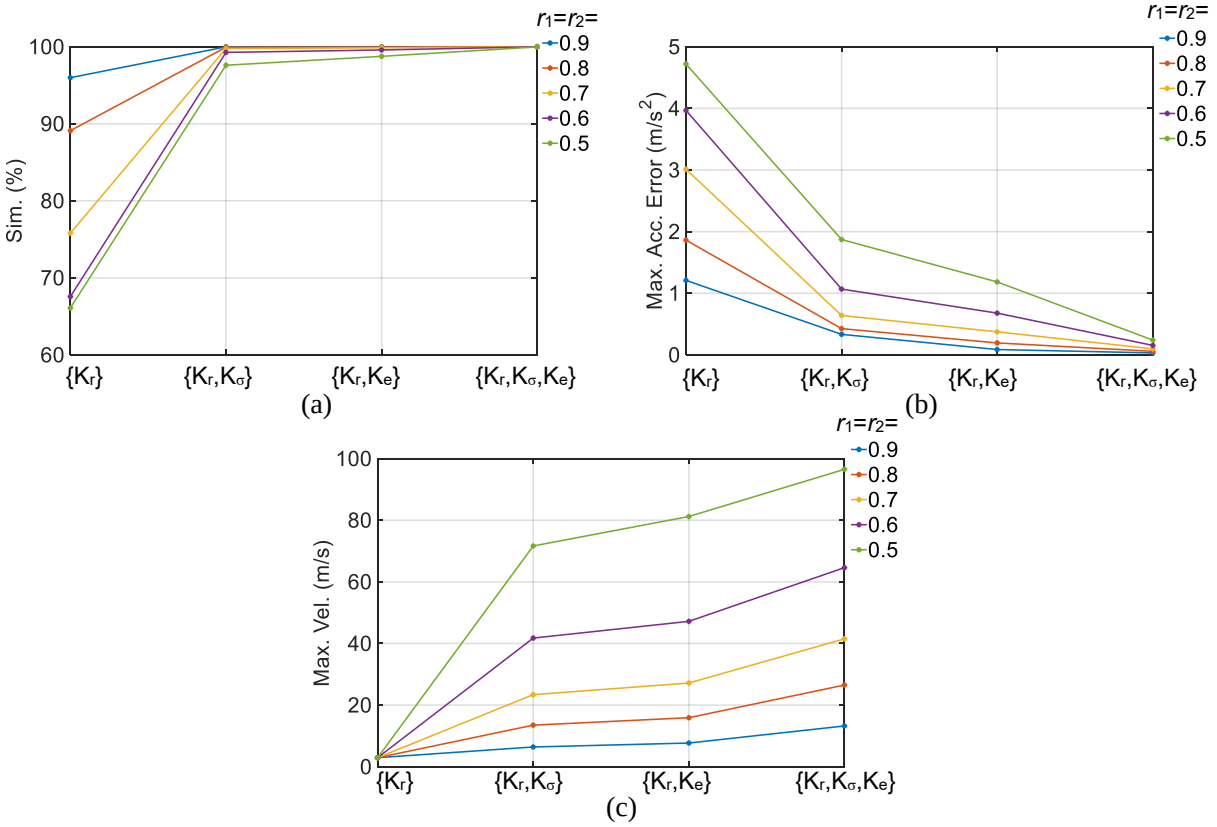

Fig. 6. Numerical results: (a) similarity, (b) maximum acceleration error, (c) required maximum velocity of the shake table.

is required to generate lager velocity as the nonlinear characteristics become stronger. The required maximum velocity for the reproduction is unrealistic to E-Defense, because its limitation of velocity is 2.0 m/s. This significant increase in the required velocity is mainly because the nonlinearity characteristics in the amplification device causes to lose its amplifying effect and the shaking table itself has to significantly move for the compensation of the loss.

4. Conclusions

In this study, we numerically examined the performance of NSBC for a shaking table with a double-layer amplification device. The numerical simulations were performed on the base of experimental conditions of the E-Defese test that had been performed in 2007 for a high-rise building under a long period ground motion. In the numerical simulations, a type of nonlinear springs was incorporated into the amplification device to more precisely demonstrate the characteristic observed in the amplification device of the E-Defense test. Then, four types of practices of NSBC were examined in the numerical simulations. As a matter of course, the simplest practice relying only on the feedback action $\{K_r\}$ was found to ineffective to the device having severe nonlinearity. Practices using one of feedback actions of nonlinear signal or error signal, which corresponds to the practices $\{K_r, K_\sigma\}$ and $\{K_r, K_e\}$, were effective to such nonlinearity. The practice using both feedback actions archived the most accurate control of the amplification device even with severe nonlinearity. In terms of control accuracy, NSBC was found to be effective to accurately control the amplification device. However, this study revealed that systems having some strong nonlinearity is not suitable as the amplification device, because such nonlinearity simply increases the effort of the shaking table. Thus, the amplification device to be placed on a shaking table needs to be carefully designed to maximum its amplification effect.

5. References

[1] Nakashima M, Nagae T, Enokida R, Kajiwara K. Experiences, accomplishments, lessons, and challenges of E-defense-Tests using world's largest shaking table. *Japan Architectural Review* 2018; 1(1): 4–17. DOI: 10.1002/2475-8876.10020.

[2] Ji X, Kajiwara K, Nagae T, Enokida R, Nakashima M. A substructure shaking table test for reproduction of earthquake responses of high-rise buildings. *Earthquake Engineering and Structural Dynamics* 2009; 38(12): 1381–1399. DOI: 10.1002/eqe.907.

[3] Enokida R, Kajiwara K, Nagae T, Ji X, Nakashima M, Development of shaking table experiment method to reproduce responses of high-rise buildings under ground motion. *Journal of Structural and Construction Engineering (Transactions of AIJ)* 2009; 634, 2111–2117.

[4] Enokida R, Nagae T, Kajiwara K, Ji X, Nakashima M, Development of shaking table test techniques to realize large response and evaluation of safety of a high-rise building. *Journal of Structural and Construction Engineering (Transactions of AIJ)* 2009; 637, 467–476.

[5] Tagawa Y, Tu JY, Stoten DP. Inverse dynamics compensation via "simulation of feedback control systems." Proceedings of the Institution of Mechanical Engineers Part I: Journal of Systems and Control Engineering 2011; 225(1): 137–153. DOI: 10.1243/09596518JSCE1050.

[6] Enokida R, Takewaki I, Stoten D. A nonlinear signal-based control method and its applications to input identification for nonlinear SIMO problems. *Journal of Sound and Vibration* 2014; 333(24): 6607–6622. DOI: 10.1016/j.jsv.2014.07.014.

[7] Enokida R. Stability of nonlinear signal-based control for nonlinear structural systems with a pure time delay. Structural Control and Health Monitoring 2019; 26(8): e2365. DOI: 10.1002/stc.2365.

[8] Enokida R, Kajiwara K. Nonlinear signal-based control for single-axis shake tables supporting nonlinear structural systems. *Structural Control and Health Monitoring* 2019; 26(9): e2376. DOI: 10.1002/stc.2376.

